 doi:10.20944/preprints202205.0170.v2

Article

Reliable Machine Learning for the Shear Strength of Beams Strengthened Using Externally Bonded FRP Jackets

Moamen Gasser [1], Omar Mahmoud [2] , Taha Elsayed[3] and Ahmed Deifalla [4, *]

1. Engineer, Future University in Egypt; moamen.hassan@fue.edu.eg.
2. Assistant professor, Future University in Egypt; omar.saad@fue.edu.eg.
3. Associate professor, Benha university, taha.ibrahim@feng.bu.edu.eg.
4. Full professor, Future University in Egypt; ahmed.deifalla@fue.edu.eg.

* ahmed.deifalla@fue.edu.eg; Cell: (+2) 01021490978-Phone: (202) 26186100 Ext 1408-Fax: (202) 26186111.

Abstract: All over the world, shear strengthening of reinforced concrete elements using external fiber-reinforced polymer jackets could be used to improve building sustainability. However, reports issued by the American Institute for concrete called for heavy scrutinizing before actual field implementation. The very limited number of proposed shear equations lacks reliability and accuracy. Thus, further investigation in this area is needed. In addition, machine learning techniques are being implemented successfully in developing strength models for complex problems including shear, flexure, and torsion. This study aims to provide a reliable machine learning model for reinforced concrete beams strengthened in shear using exterally reinforced fiber polymer sheets. The proposed model was developed and validated against the experimental database and the very limited models in the literature. The model showed better agreement with the experimentally measured strength compared to the previous models.

Keywords: Shear Strength; FRP; Anchorage devices; effective FRP strain

1. Introduction

Significant shear act upon reinforced concrete (RC) elements in many buildings. Various shear failures of RC buildings were reported [1]. The shear failure of RC beams is brittle [2-5]. The elevated cost of replacing infrastructure has driven research into several strengthening techniques. Shear strength is vital in lots of projects [6-8]. The fiber-reinforced polymer (FRP) sheets have various benefits over steel plates. Thus, research has been conducted to investigate the behavior of FRP externally and internally RC beams [9-11]. FRP has been used fruitfully in the automotive and aerospace industries for a few decades. It has been used for new structural elements in recent years, particularly in aggressive environments including but not limited to chemical plants, which is because its being corrosion free [12-14]. FRP can be used in situations where the usage of steel would be impossible or impractical [15-16]. For instance, it can be formed on-site to fit any irregular shape. FRP fabrics can be wrapped around curves (i.e., beams' sides, columns' corners, or beams' soffits). It is lighter in weight than steel with the same strength [17]. It is easy to handle and cut into the required length.

 doi:10.20944/preprints202205.0170.v2

Worldwide, there is a lack of consensus on the shear strength contribution of the externally bonded (EB)-FRP jackets. Several design guidelines and codes exist worldwide [18-22]. This lack is due to the following reasons:

- The shear strength and mechaism is complicated;
- For several EB-FRP strengthening schemes, the premature debonding failure is difficult to predict;
- The EB-FRP is linear up to failure, while no yield is observed;
- The interaction between the concrete, internal steel reinforcements, and the EB-FRP reinforcement.

In addition, The shear strengthening using EB-FRP can be executed in different patterns:

- Full wrapping the sheets around the cross-section (fully jacket);
- Bonding L-shaped EB-FRP sheets to the bottom or the sides of the cross-section (U-jacket);
- Bonding EB-FRP sheets to the sides of the cross-section (side jacket).

The sheets can be adhesively bonded in a continuous or discrete configuration. However, both U-jacket and side-jaket schemes are vulnerable to premature debonding failure, which occurs once a critical shear crack opens and widens. In case the EB-FRP bonded length is not adaquate to provide anchorage for the transfer of the tensile force bewtween the FRP and the concrete. Thus, the EB-FRP fails by premature debonding. Which can be prevented using appropriate anchorage devices.

The beams' shear strength of EB-FRP beams can be calculated as the summation of the shear resistance of the transverse steel (if any), the concrete, and the EB-FRP. In addition, Several guidelines add the resistance of the EB-FRP to the shear capacity of the un-strengthened element [18-22]. However, previous studies have shown that EB-FRP jackets will affect the effective stress level of internal steel. Thus, this superposition approach could lead to nonconservative results [23-27]. This lack of conservative could be because it changes concrete diagonal cracking, the diagonal strut orientation, or the transverse reinforcement stress.

 doi:10.20944/preprints202205.0170.v2

The engineering community is increasingly using EB-FRP systems to improve the strength of existing RC beams. Recent research studies have lead to a worldwide execution this technique. However, debonding of EB-FRP sheets has been a main issue for EB-FRP RC beams in shear and torsion. For EB-FRP RC beams, premature failure by EB-FRP debonding is generally a sudden type of failure. Therefore, for EB-FRP RC beams, debonding is an unwanted failure mode. There are two types of EB-FRP debonding were observed by Deifalla [17], namely, end or intermediate debonding, as shown in Figure1, which is due to either cover spalling or concrete cracking.

The anchorage systes of EB-FRP jackets has no rational and reliable design rules. Thus, FRP design codes and guidelines specify that physcial experimental testing should conducted as a supllement for the implementation of these techniques [18-22]. However, the procedure of these experimnetal testing is not spcified by existing guidelines and design codes [26-28]. In addition, Due to the limited time schedule and the budget constraints of projects, it is rarely a possibility to perform such testing. Thus, the potential benefits of FRP anchorages are usually subistituted by using additional increase in the EB-FRP, which is not economic. The experimental studies condcuted in this area are limited by case dependency and usually using a small ascle model; thus, it has a small impact on the understanding of the behavior.

The contribution of EB-FRP to the resistance of RC beams is affected by EB-FRP type, direction, arrangement, and allocation. The efficacy of EB-FRP is boosted by attaching the EB-FRP in a direction parallel to the maximum tension stress. Therefore, EB-FRP arrangements change the shear capacitiy of strengthened RC beams. A Comprehensive research investigations on the shear strength of EB-FRP-RC beams is rare, and many queries regarding the mechanisms involved are not yet settled. With the following exception, many researchers have porposed idealized models similar to that used for the internal steel stirrups, which is only valid if the shear contribution of EB-FRP comes from the tensile fiber capacity at a strain close to the ultimate tensile strain of the EB-FRP.

If full FRP wrapping is not feasible, to achieve the full design capacity, anchorage systems can be used for EB-FRP strengthened beams using FRP [29-30]. The European fib [18] code suggest that anchorage

 doi:10.20944/preprints202205.0170.v2

systems be at the compressive zone of the EB-FRP-RC beams. However, no further details were provided. On the other hand, the ACI [21] indicated that anchorage systems at the termination points of EB-FRP, which will produce larger tension stress transfer. However, the efficiency of these anchorage systems and the the developed level of tensile stress before failure should be validated using experimental testing of a scaled model before excution [21]. In a study by Mofidi [29-31], it was concluded that experimental testing are needed to validate the proposed anchorage factors for the end-anchorage systems. Kalfat [32] demonstrated the validaty of upgrading the shear strength due to anchoring systems for EB-FRP materials. However, there remains a lack of enough work in this area. A more recent review by Godat [33] has shown that further research is essential to enhance the reliability of the shear strength predictions of EB-FRP-RC beams. The interaction between the FRP shear strength, strain, and parameters are required for robust design equations.

Machine learning is being implemented in various applications because it can capture the actual behavior for complex problems involving many parameters [34]. This research investigation aims at developing a reliable and accurate strength model based on advanced machine learning techniques. An extensive database was collected and used to train and validate the model, as shown in figure 2. A machine learning model was developed and compared with available models from the literature. Concluding remarks were outlined.

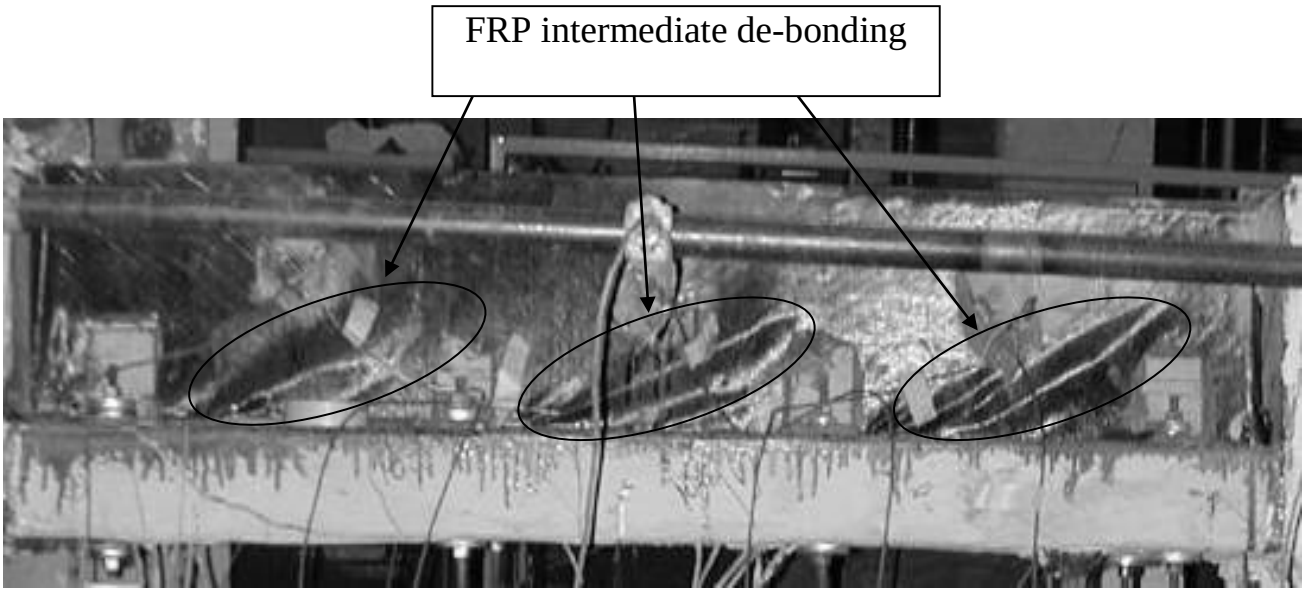

 doi:10.20944/preprints202205.0170.v2

(a)

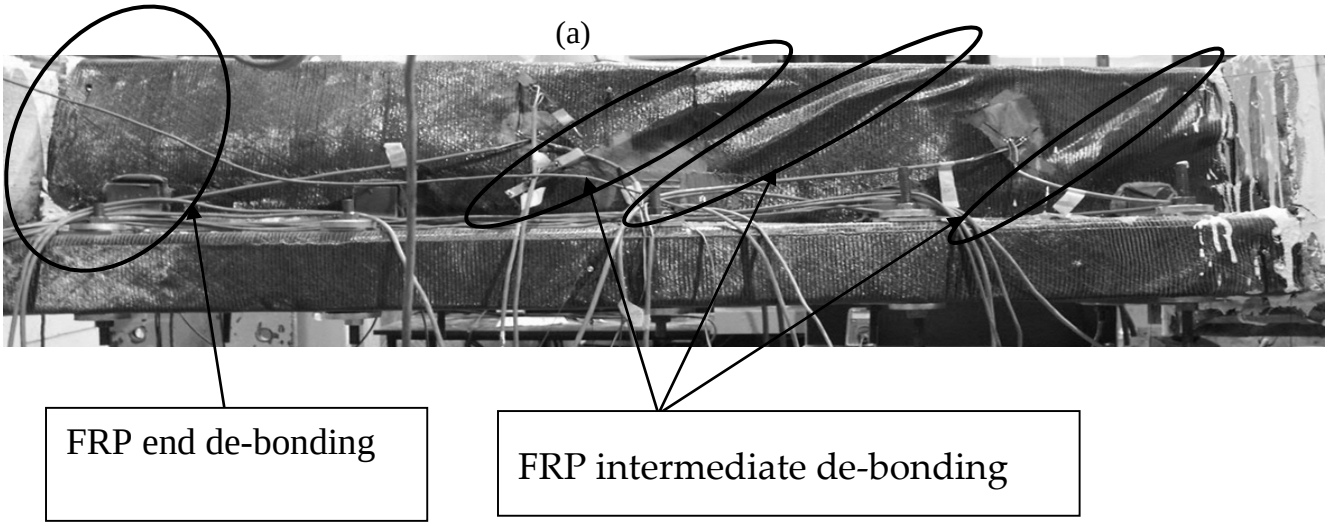

(b)

Figure 1. FRP end and intermediate debonding.

2. Previous Studies

Relatively limited detailed studies have investigated the shear strength of RC members; in addition, many questions regarding the strength mechanism, especially the usage of anchorage devices, are yet to be resolved. Many researcher studies have idealized the EB-FRP jacket in a manner similar to that of steel

 doi:10.20944/preprints202205.0170.v2

shear reinforcments, assuming that the contribution of EB-FRP to shear capacity arises from the EB-FRP capacity to resist tensile stresses at a strain, which is less than or equal to the FRP ultimate tensile strain [16-18]. Numerous experimental tests was conducted out in this field of research, and existing design codes and guidelines are available for designing EB-FRP elements [18-22]. Both empirical evidence and code suggest a performance enhancement can be attained by using EB-FRP; however, more detailed work is required to quantify their contribution to the strength of the beams under shear [18-22]. Many parameters influence the effective FRP strain for shear strengthened RC members, including but not limited to: (1) The type of fibers in terms of Young's Modulus; (2) The fiber orientation in terms of the inclination angle to the beam longitudinal axis; (3) The fiber distributions in terms of the number of plies and thickness of the FRP fabrics; (4) The FRP bond schemes in terms of the sides the FRP is bonded to (i.e., side bonding; U-jacket; full wrapping); (5) The concrete compressive strength; and (6) The usage of anchorage devices.

Preprints (www.preprints.org) | NOT PEER-REVIEWED | Posted: 23 August 2022 doi:10.20944/preprints202205.0170.v2

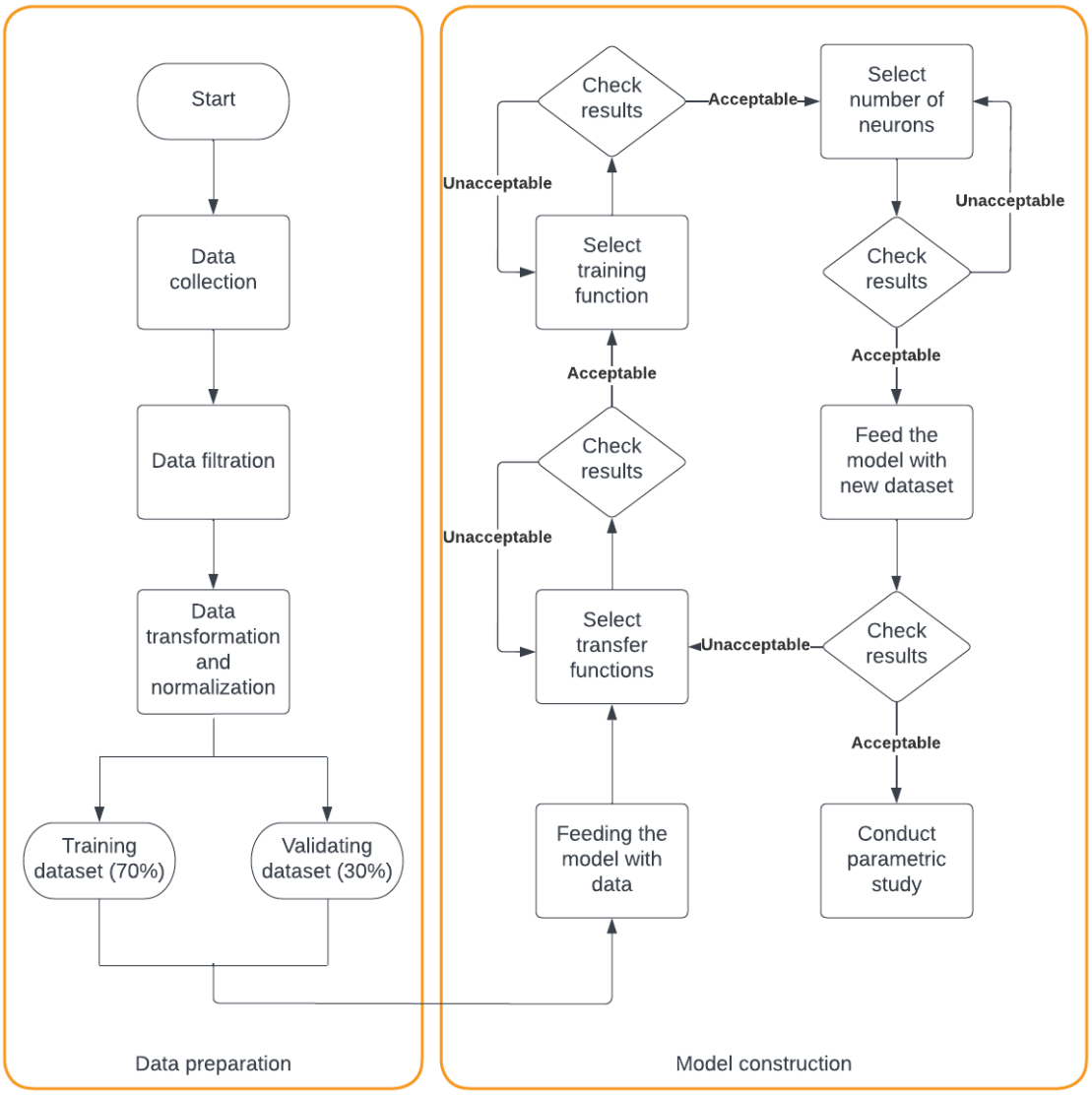

Figure 2. Work scheme.

3. Experimental database

An extensive database of 200 beams was strengthened using an EB-FRP jacket under shear collected from the literature. The database contains results from more than 80 experimental studies. In addition, this database includes Eb-FRP beams available in the literature [27, 35-37]. Although the data is available in existing databases, all data was validated using the original study.

Collected parameters were related to the beam and the FRP jacket as follows: Width of beam cross-section (X1), beam height (X2), the effective depth of beam cross-section (X3), beam span (X4), shear span

Preprints (www.preprints.org) | NOT PEER-REVIEWED | Posted: 23 August 2022 doi:10.20944/preprints202205.0170.v2

to depth ratio (X5), concrete compressive strength (X6), steel flexure reinforcement ratio (X7), and steel shear reinforcement ratio (X8), strength technique (X9), FRP jacket height (X10), the width of FRP jacket (X11), the thickness of FRP jacket (X12), spacing between FRP strips (X13), FRP reinforcement ratio (X14), angle of fiber orientation (X15), ultimate stress of FRP (X16), FRP young's modulus (X17), and FRP rupture strain (X18), and Shear strength in kN (X19). Table 1 shows the statistical measures for all parameters.

Table 1. Statistical measures for all parameters.

	Minmum	Maximum	Average	Stdev.
X1	70	600	189	84
X2	102	720	336	119
X3	85	660	291	107
X4	600	6400	2205	1012
X5	1.3	6.9	2.85	0.74
X6	4	63.4	27.37	11.16
X7	0.75	7.54	2.89	1.41
X8	0.02	0.84	0.10	0.14
X10	89	720	319	121
X11	1	300	47	75
X12	0.044	4000	223	575
X13	1	500	99	134
X14	0.0029	0.0895	0.0042	0.0084

Preprints (www.preprints.org) | NOT PEER-REVIEWED | Posted: 23 August 2022 doi:10.20944/preprints202205.0170.v2

X15	20	90	80	19
X16	112	4840	3112	1108
X17	5	392	202	85
X18	6.6	47.4	16.6	6.3
X19	3	494	69	64

3. Parameters selection

Pearson parametric method was used to determine the influence of beam details on the FRP shear strength, as shown in figure3. The selected parameters included X1, X2, and X3, while parameters X4, X5, X6, X7, and X8 were not chosen as they have a lower Pearson coefficient. For a more efficient and faster training and validating process, the input parameters have been normalized to be between 0 and 1, according to equation 1. While FRP's shear strength (model's output) has been transformed according to equation 2 for better output distribution, as shown in figure4.

- $X_{i,norm} = \frac{X_i - X_{avg}}{X_{max} - X_{min}}$ 1. (1)

b)

where i is the number index for each input parameter, $X_{i,norm}$ is the normalized value for the input parameter, X_i is the value of the input parameter before normalization, Xavg is the average of the parameter X_i, X_{max} and X_{min} are the values of the maximum and minimum values of the input parameter X_i.

- $S^T = ln(S + 1)$ 2. (2)

where S is the value of the added shear strength by FRP in kN while S^T is its transformed value, the input parameter for the proposed model data has been filtered and transformed to follow a normal distribution curve for a better training process to build the model has been as shown in figure 4.

 doi:10.20944/preprints202205.0170.v2

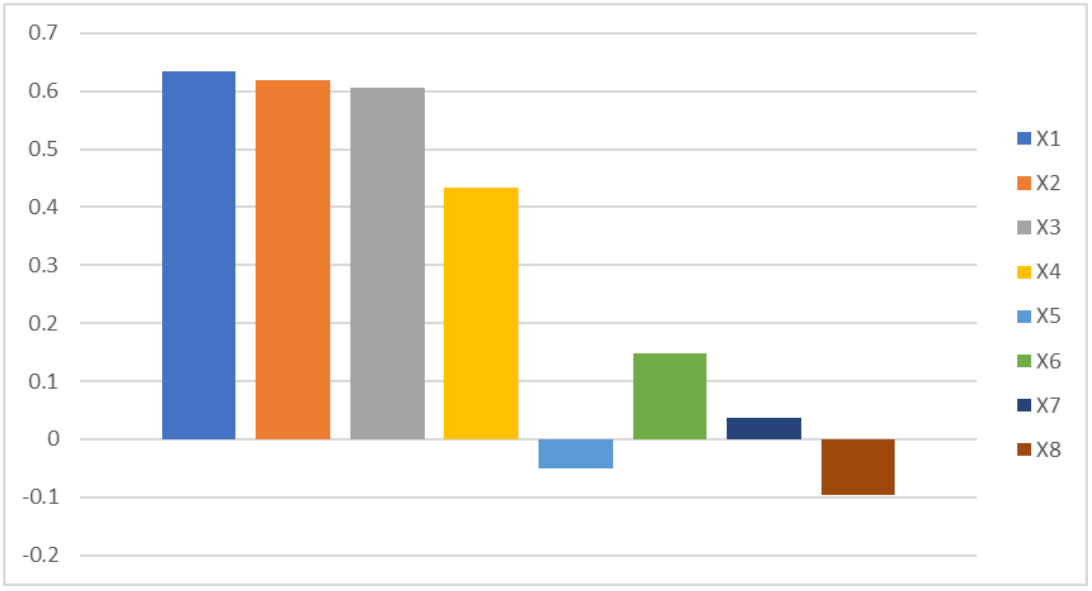

Figure 3. Results of Pearson variables study on FRP shear strength.

 doi:10.20944/preprints202205.0170.v2

b)

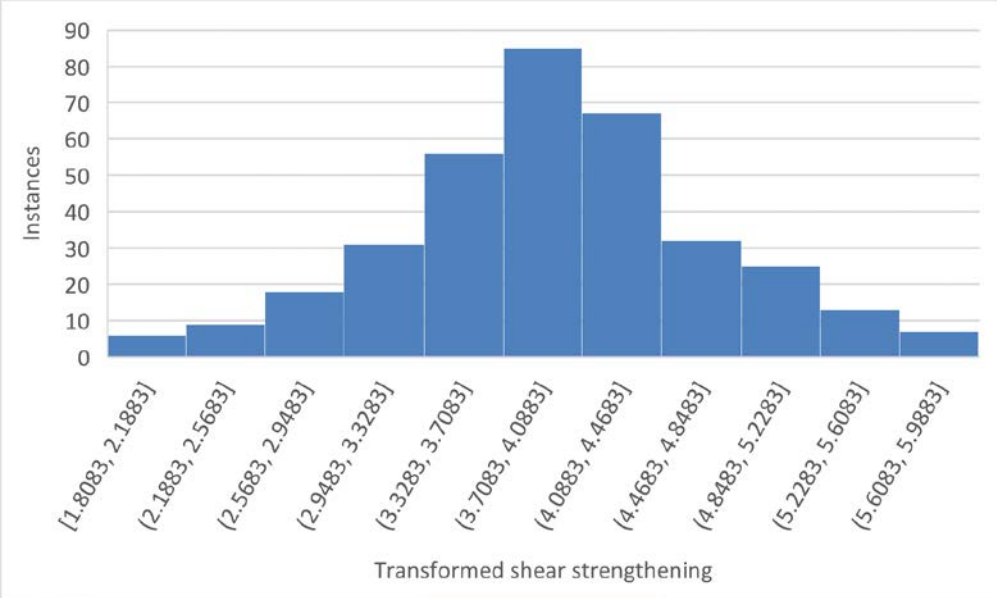

Preprints (www.preprints.org) | NOT PEER-REVIEWED | Posted: 23 August 2022 doi:10.20944/preprints202205.0170.v2

Figure 4. Distribution of the failure shear force a) before and b) after transformation.

4. Model development

A script has been developed to generate more than 6750 different artificial neural networks (ANN) models to compare and boost the developed model performance using MATLAB. In addition, different combinations of various parameters have been tested as shown if figure 5.

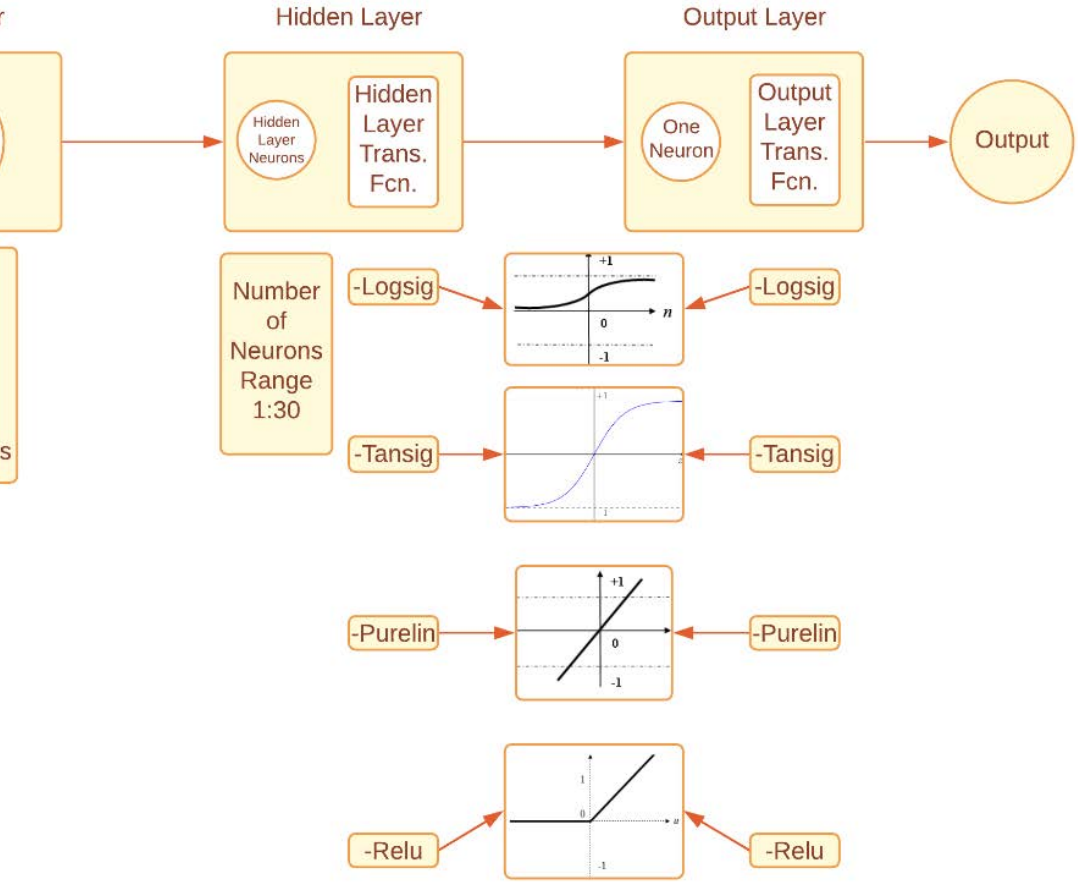

Figure 5. Combination of different model parameters.

During the model construction, the transfer function of the hidden and output layers were the first parameters to be determined. Then, the training function and the number of neurons in the hidden were

Preprints (www.preprints.org) | NOT PEER-REVIEWED | Posted: 23 August 2022 doi:10.20944/preprints202205.0170.v2

optimized by plotting the number of neurons versus the correlation coefficient (R^2) and root mean square error (RMSE) in figures 6 and 7.

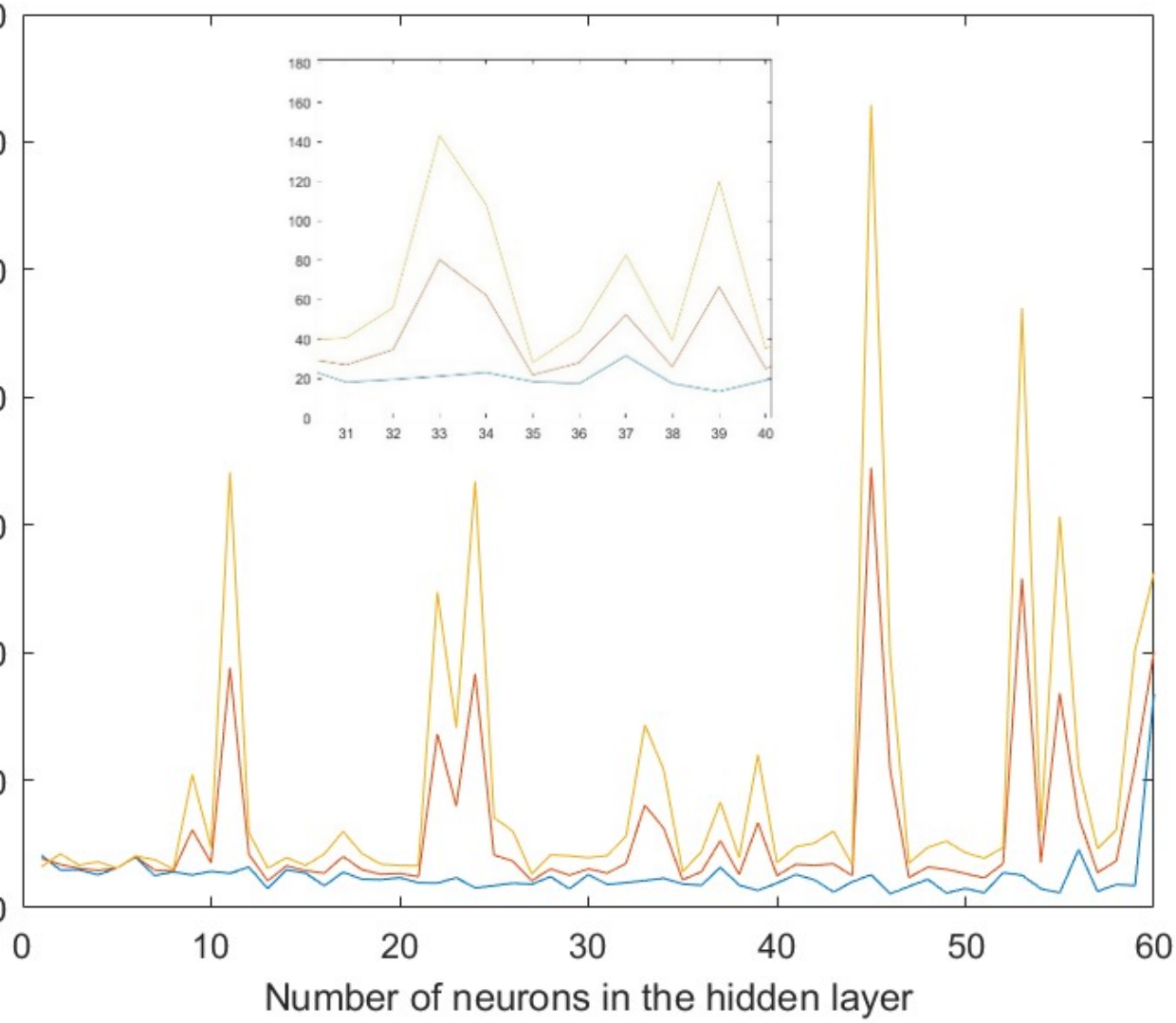

Figure 6. Neurons number in hidden layer versus RMSE.

Preprints (www.preprints.org) | NOT PEER-REVIEWED | Posted: 23 August 2022 doi:10.20944/preprints202205.0170.v2

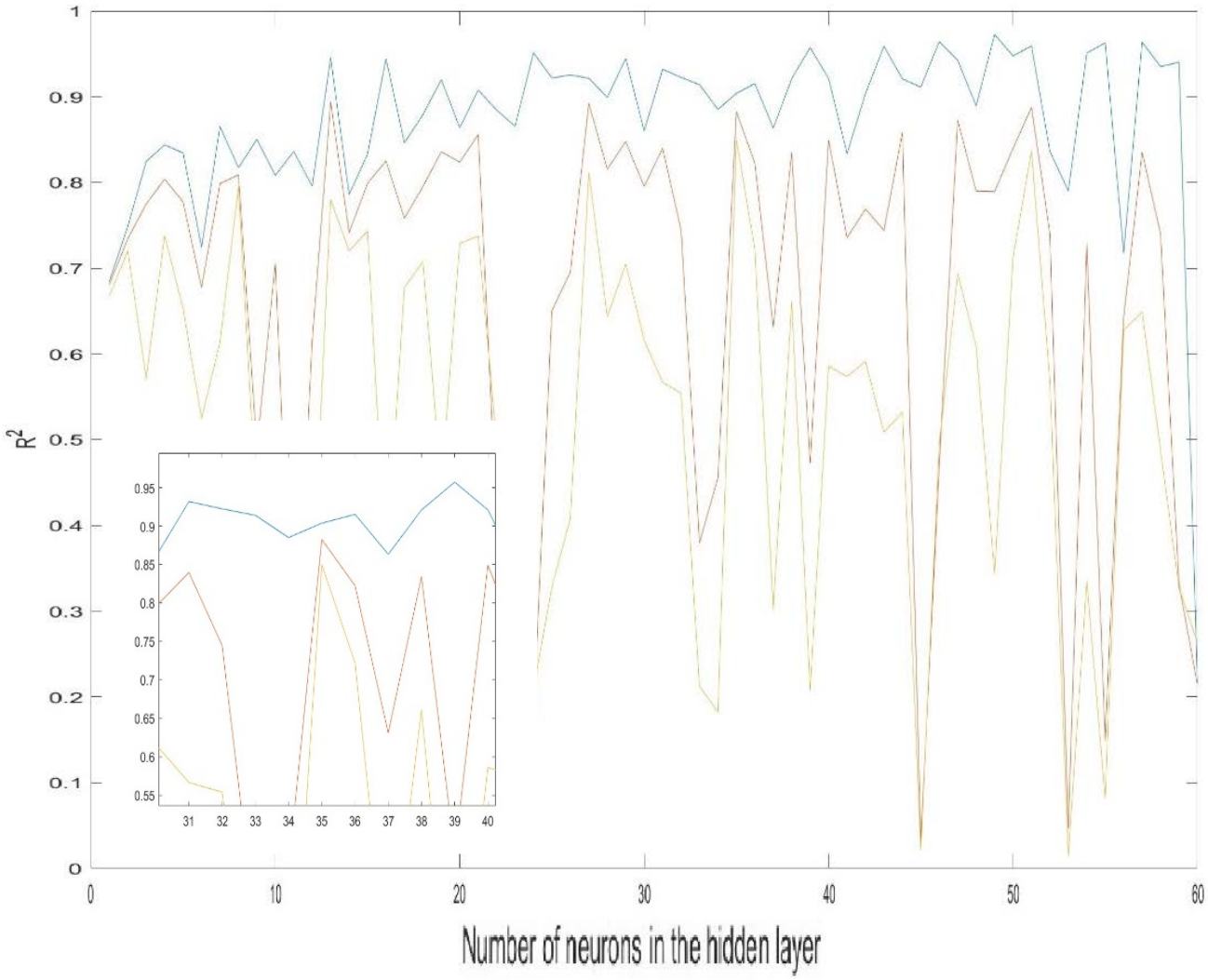

Figure 7. Neurons number in the hidden layer versus R^2.

The number of neurons was optimized to be 35 neurons in the hidden layer, while the transfer functions were TANSIG and PURELIN for the hidden and the output layers, respectively figure 8. Based on the constricted model, a mathematical equation has been developed to predict the shear strength added by FRP equation 3.

Preprints (www.preprints.org) | NOT PEER-REVIEWED | Posted: 23 August 2022 doi:10.20944/preprints202205.0170.v2

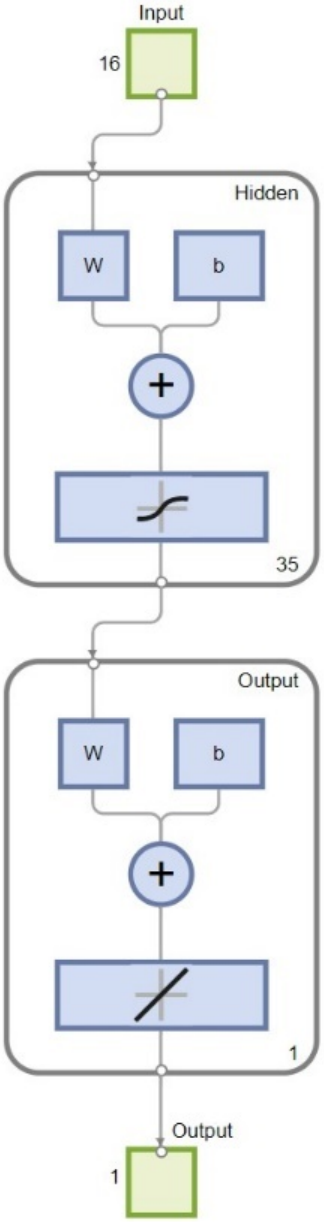

Figure 8. The proposed ANN model architecture.

- $S = Exp\left[PURELIN\left[\sum_{i=1}^{N} W_{2i} TANSIG\left(\sum_{j=1}^{J} W_{1j} \times \frac{X_j - X_{avg}}{X_{max} - X_{min}} + b_{1i}\right)\right] + b_2\right] - 1$ (3)

where Exp is the exponential function, N is the number of neurons in the hidden layer, which has been optimized to be 35 neurons, W2i is the weight of the output layer, J is the number of input variables, W1 is the weight of the hidden layer, Xj is the value of the input variable (strength configuration, X1, X2, X3, X9,

Preprints (www.preprints.org) | NOT PEER-REVIEWED | Posted: 23 August 2022 doi:10.20944/preprints202205.0170.v2

X10, X11, X12, X13, X14, X15, X16, X17, and X18) b1 is the bias of the hidden layer, and b2 is the bias of the output layer.

In which, the values of the input parameters go through the input layer to be multiplied by the weights that connect the input layer with the hidden layer. The bias of the first layer is added to the multiplication results before they transform through the activation function of the hidden layer (TANSIG). The outcome of the transfer function is then multiplied by the weights of the output layer and added to the bias of the hidden layer. Finally, the product goes through the output layer's transfer function (PURELIN) to give the predicted value of the shear strength in KN.

Later, the performance of the ANN model was boosted by 1000 epochs; the best model outcome was found to be at the 8th epoch, then the validation check stopped the training process at the 14th epoch, as shown in figure 9.

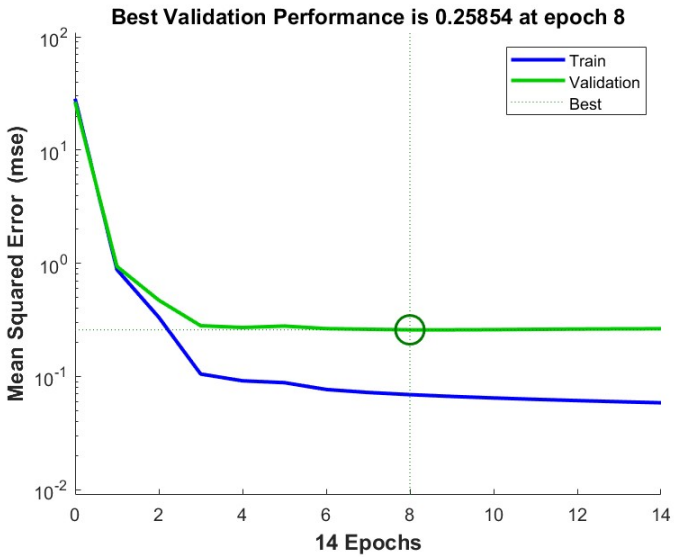

Figure 9. Epochs versus Mean square error.

5. Model validation

After the model construction, the model was used to predict the shear strength for FRP in KN then the predicted value was plotted versus the actual values in figure10. In addition, statistical tests have been conducted to test the accuracy of the newly developed model. Training, validating, and overall datasets have

Preprints (www.preprints.org) | NOT PEER-REVIEWED | Posted: 23 August 2022 doi:10.20944/preprints202205.0170.v2

been evaluated using average relative error (ARE), average absolute relative error (AARE), relative deviation (RD), standard deviation (SD), RMSE, and R2 according to equations 3-8. Also, a comparison between the actual and the predicted values are presented in figure 11. Moreover, the ratio between the predicted and actual values has been calculated according to equation 9 for both the training and validating datasets and presented in figure 13.

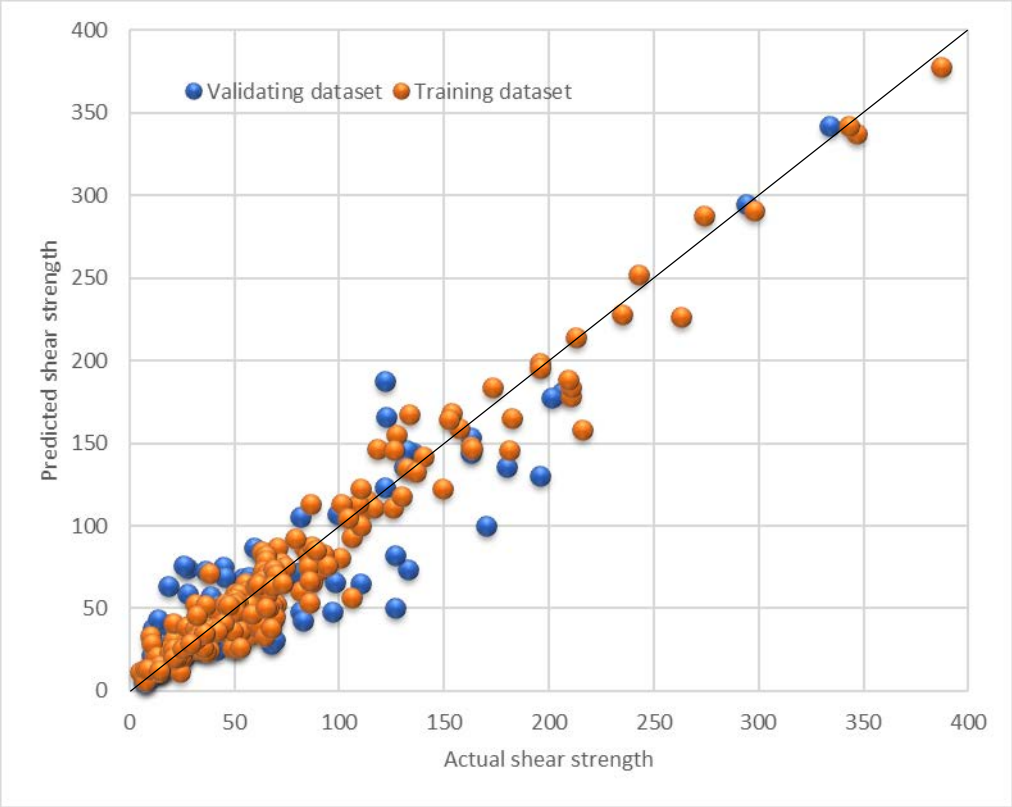

Figure 10. Actual Versus predicted shear strength value in kN.

- $$ARE = \left(\frac{1}{N} \times \sum_{i=1}^{N} \frac{S^{Predicted} - S^{Actual}}{S^{Actual}}\right) \times 100$$ 4. (4)
- $$AARE = \left(\frac{1}{N} \times \sum_{i=1}^{N} \left|\frac{S^{Predicted} - S_i^{Actual}}{S_i^{Actual}}\right|\right) \times 100$$ 5. (5)
- $$RD = \frac{S^{Predicted} - S^{Actual}}{S^{Actual}} \times 100$$ 6. (6)

 doi:10.20944/preprints202205.0170.v2

- $$SD = \left\{\frac{1}{N-1} \times \sum_{i=1}^{N}\left(\frac{S^{Predicted}-S^{Actual}}{S^{Actual}}\right)^2\right\}^{0.5}$$ 7. (7)

- $$RMSE = \left\{\frac{1}{N} \times \sum_{i=1}^{N}\left(S^{Predicted} - S^{Actual}\right)^2\right\}^{0.5}$$ 8. (8)

- $$R^2 = 1 - \frac{\sum_{i=1}^{N}\left(S^{Predicted}-S^{Actual}\right)^2}{\left(S_{Actual}^{Mean}-S^{Actual}\right)^2}$$ 9. (9)

- $$Ratio = \frac{F^{Predicted}}{F^{Actual}}$$ 10. (10)

where N is the number of tested data points, $S^{Predicted}$ is the predicted shear strength value in kN, S^{Actual} is the corresponding actual shear strength value in kN, and S_{Actual}^{Mean} is the average of the actual shear strength value in kN.

a)

Preprints (www.preprints.org) | NOT PEER-REVIEWED | Posted: 23 August 2022 doi:10.20944/preprints202205.0170.v2

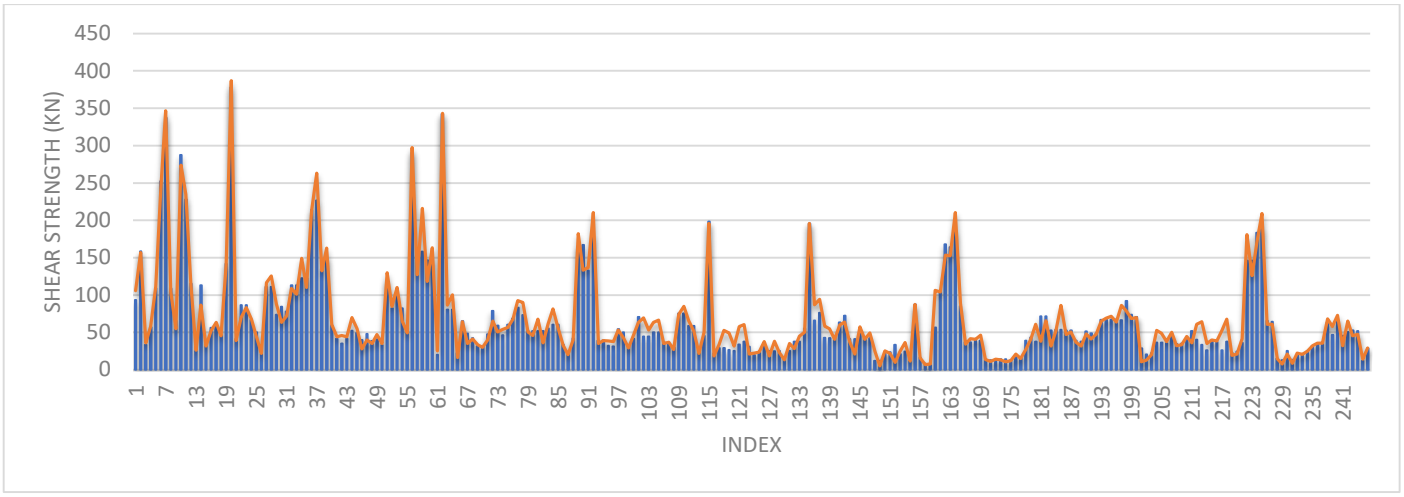

b)

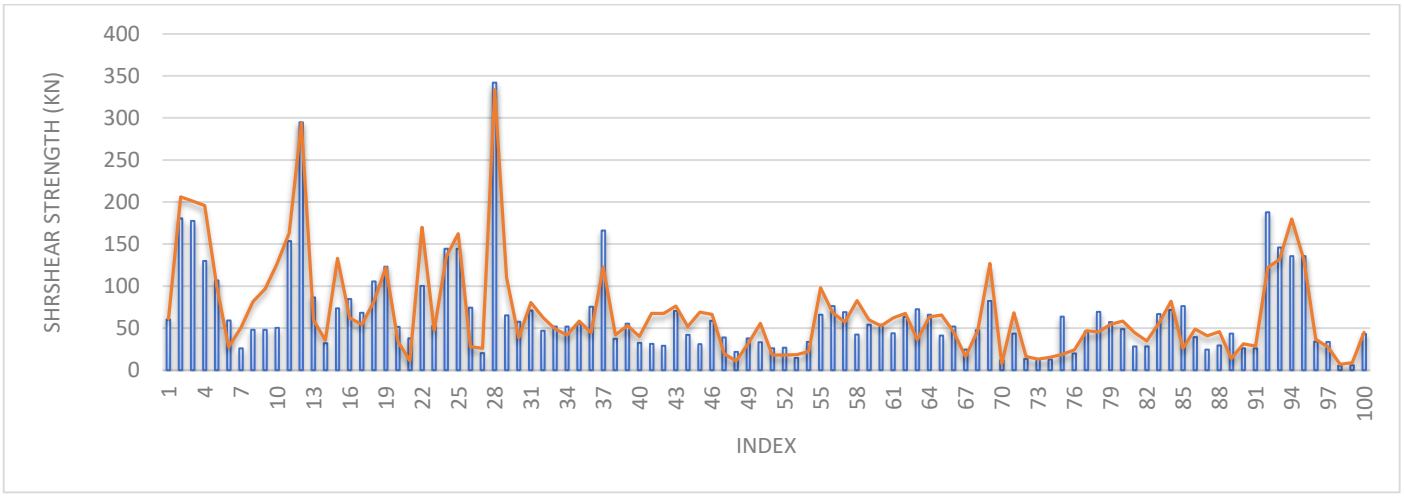

c)

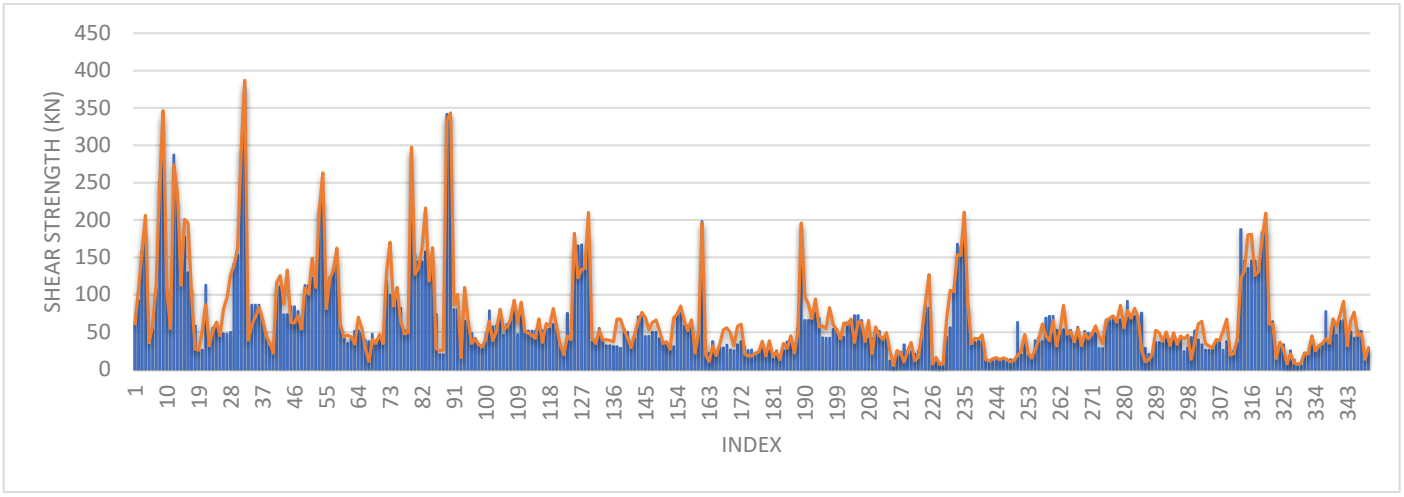

 doi:10.20944/preprints202205.0170.v2

Figure 11. Comparing the actual and predicted shear strength values in kN for a) training dataset, b) validating c) overall datasets.

Preprints (www.preprints.org) | NOT PEER-REVIEWED | Posted: 23 August 2022 doi:10.20944/preprints202205.0170.v2

a)

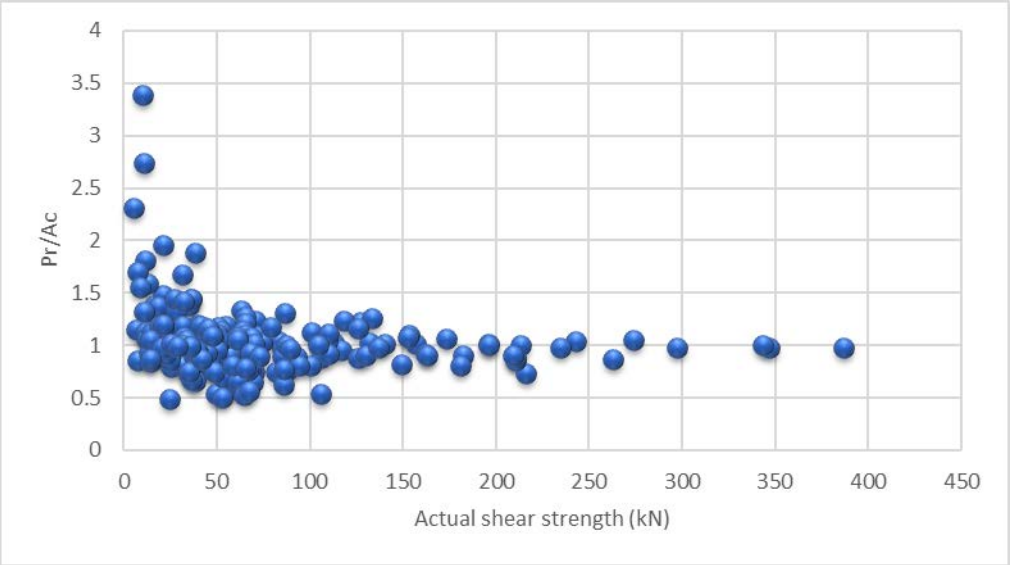

b)

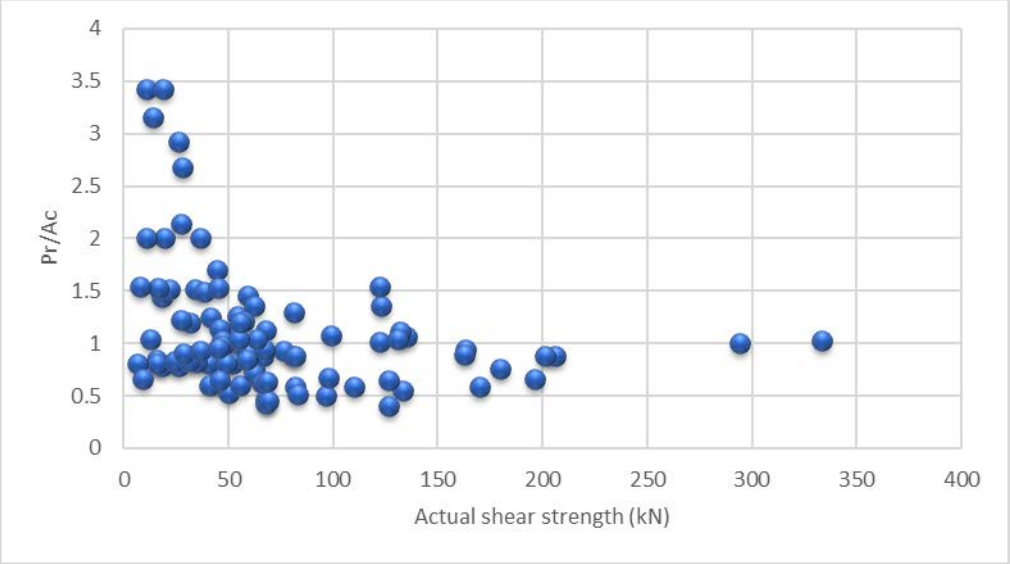

 doi:10.20944/preprints202205.0170.v2

Figure 12. The ratio between predicted to actual shear strength versus the actual shear strength value in kN for a) training dataset and b) validating dataset.

The model showed excellent performance as it has R^2 and RMSE of 0.91 and 17.45 for the overall dataset, respectively. The R^2, RMSE, ARE, AARE and SD statistical tests are summarized and listed in figures 13-17, respectivelyIn addition, the results of the different datasets were compared to check the fitting of the proposed model. While RD is plotted versus the actual shear strength and presented in figure 18.

Preprints (www.preprints.org) | NOT PEER-REVIEWED | Posted: 23 August 2022 doi:10.20944/preprints202205.0170.v2

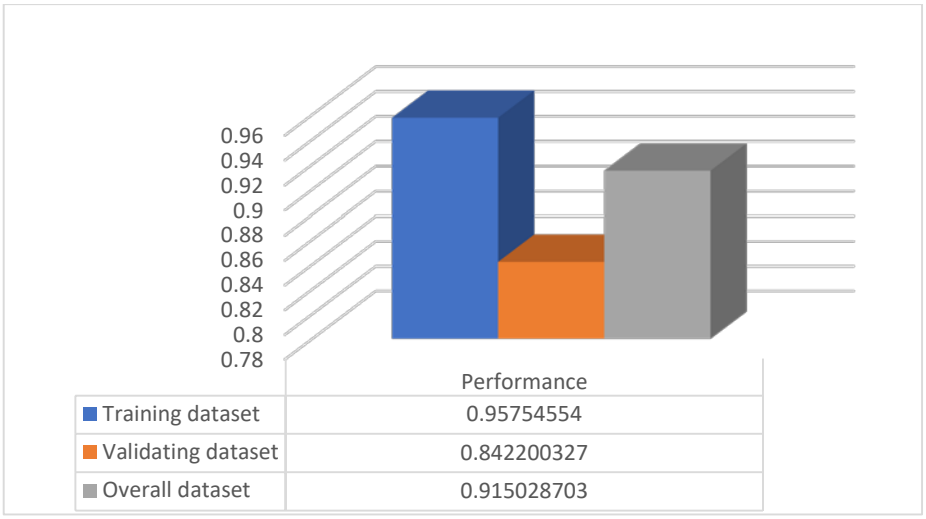

Figure 13. R^2 for training, validating, and overall datasets.

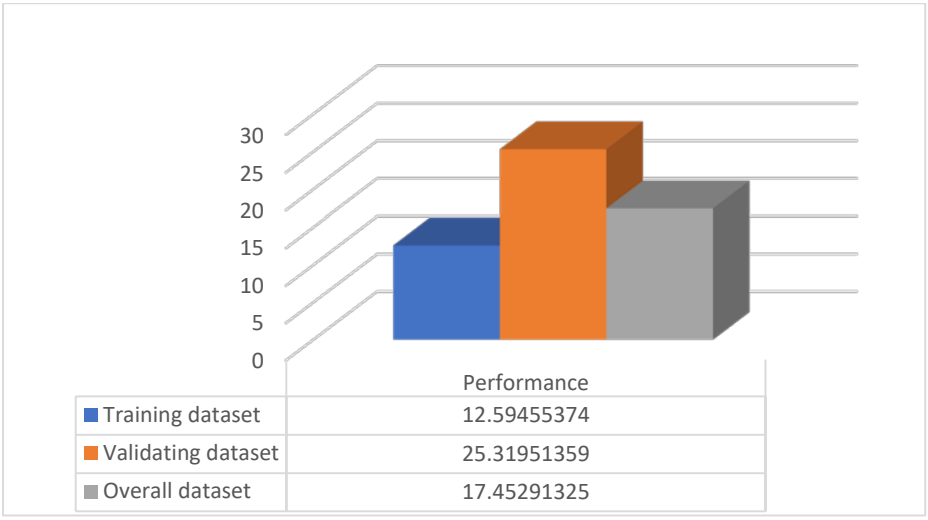

Figure 14. RMSE for training, validating, and overall datasets.

Preprints (www.preprints.org) | NOT PEER-REVIEWED | Posted: 23 August 2022 doi:10.20944/preprints202205.0170.v2

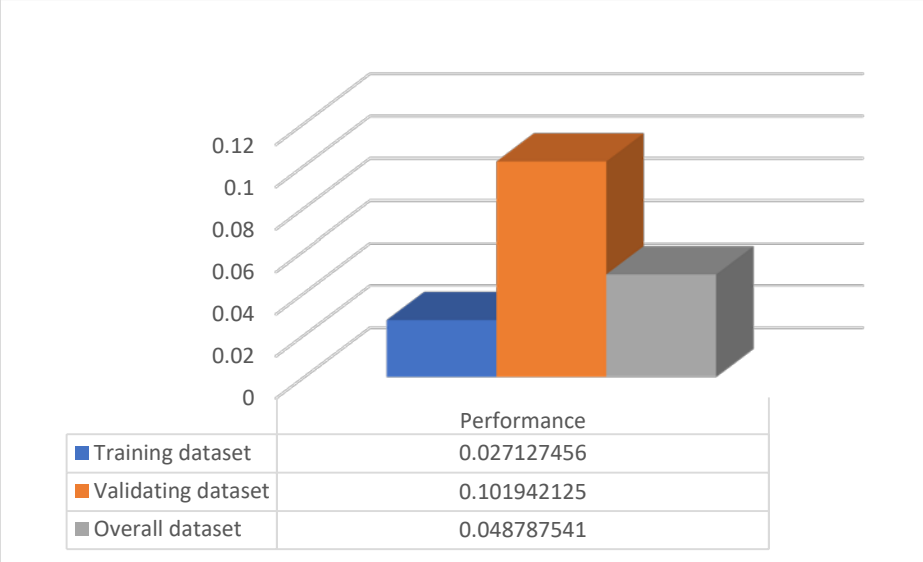

Figure 15. ARE for training, validating, and overall datasets.

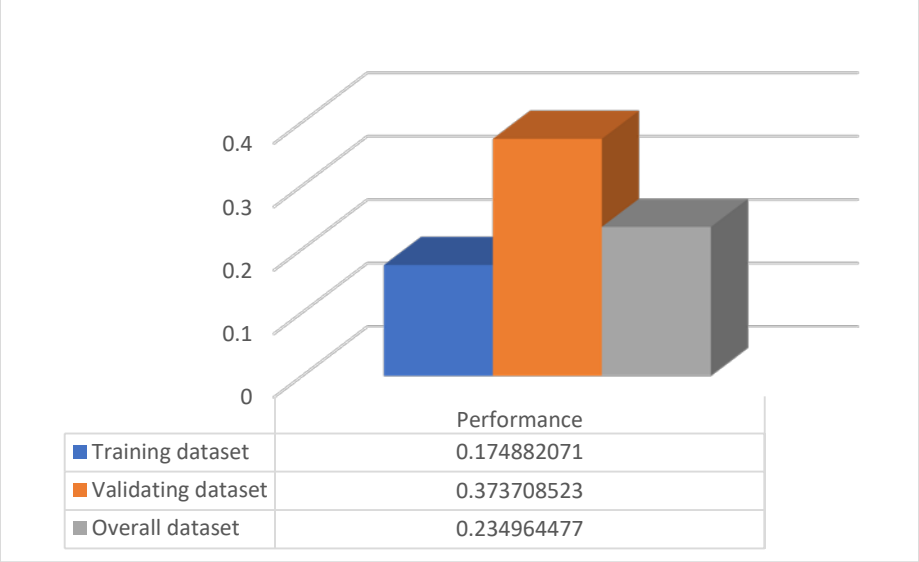

Figure 16. AARE for training, validating, and overall datasets.

Preprints (www.preprints.org) | NOT PEER-REVIEWED | Posted: 23 August 2022 doi:10.20944/preprints202205.0170.v2

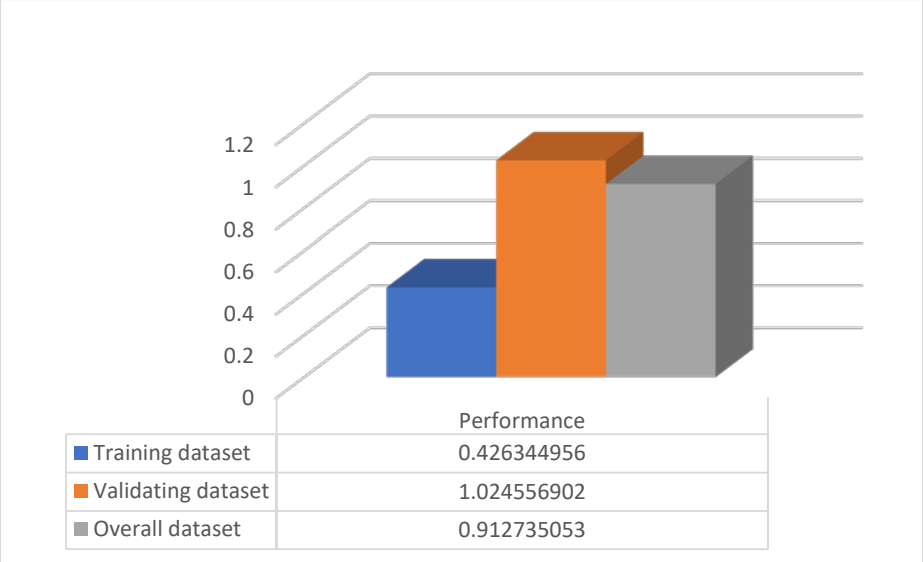

Figure 17. SD for training, validating, and overall datasets.

Preprints (www.preprints.org) | NOT PEER-REVIEWED | Posted: 23 August 2022 doi:10.20944/preprints202205.0170.v2

a)

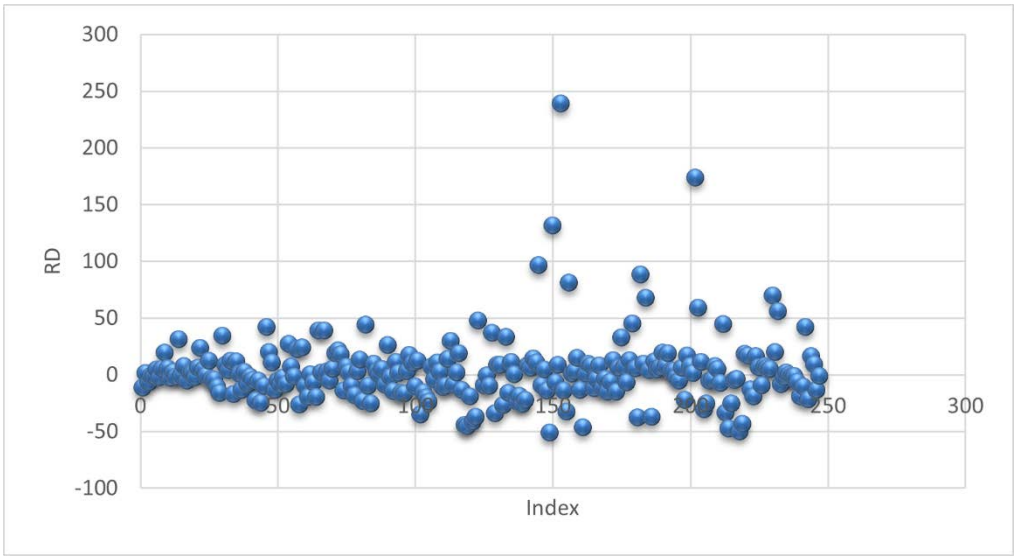

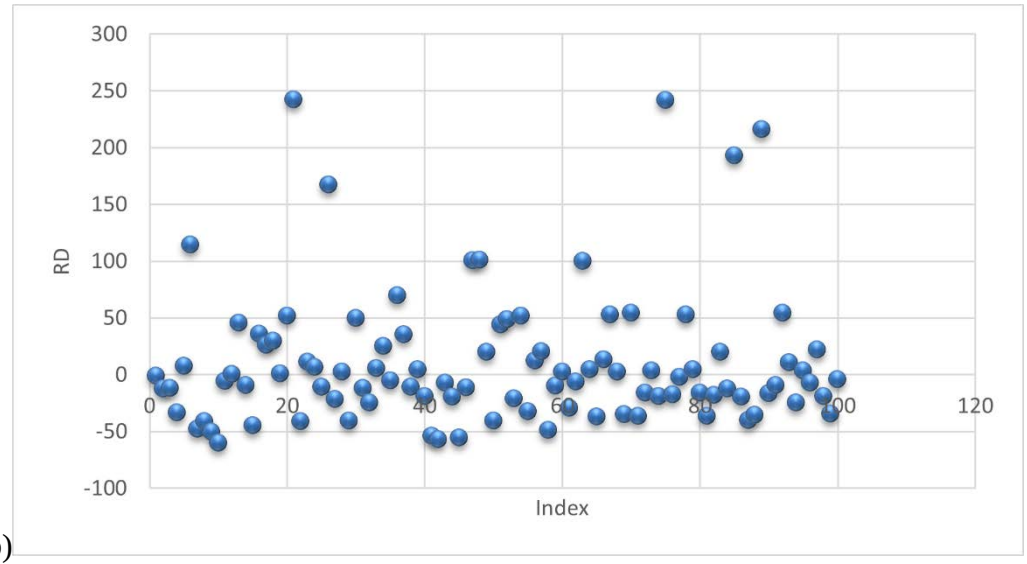

b)

Figure 18. RD versus the testing point index for a) training b) validating datasets.

After validating the model and demonstrating its credibility in predicting the shear strength value added by the FRP, the model was then used to conduct a parametric study to study the impact of each parameter individually. When investigating a certain parameter, the rest of the variables were set constant at their average value while changing the value of the tested parameter. X10, X14, X15, and X17 were investigated, and their values are plotted versus the model outcome figures 19-22.

Preprints (www.preprints.org) | NOT PEER-REVIEWED | Posted: 23 August 2022 doi:10.20944/preprints202205.0170.v2

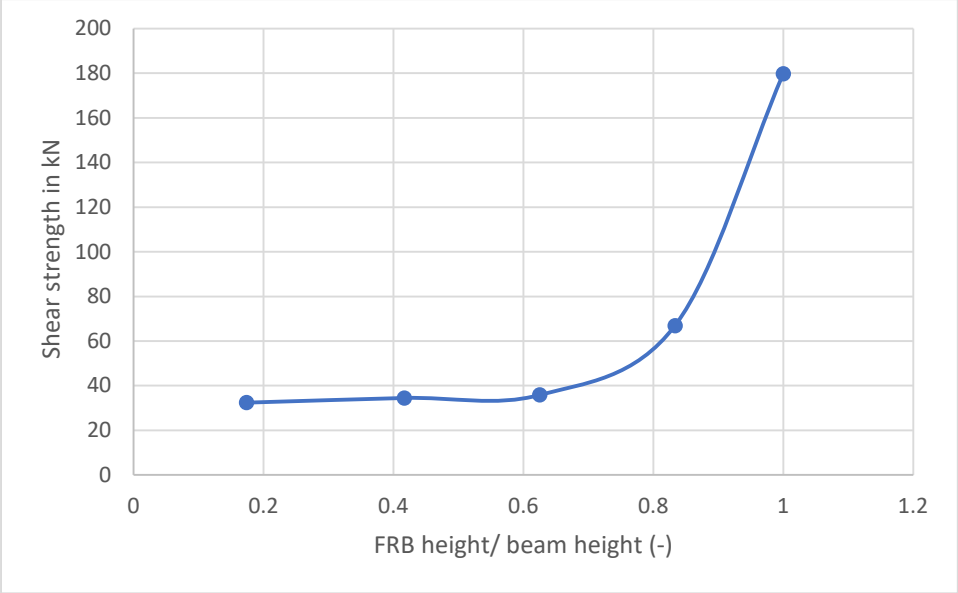

Figure 19. The effect of X10 on shear strength value.

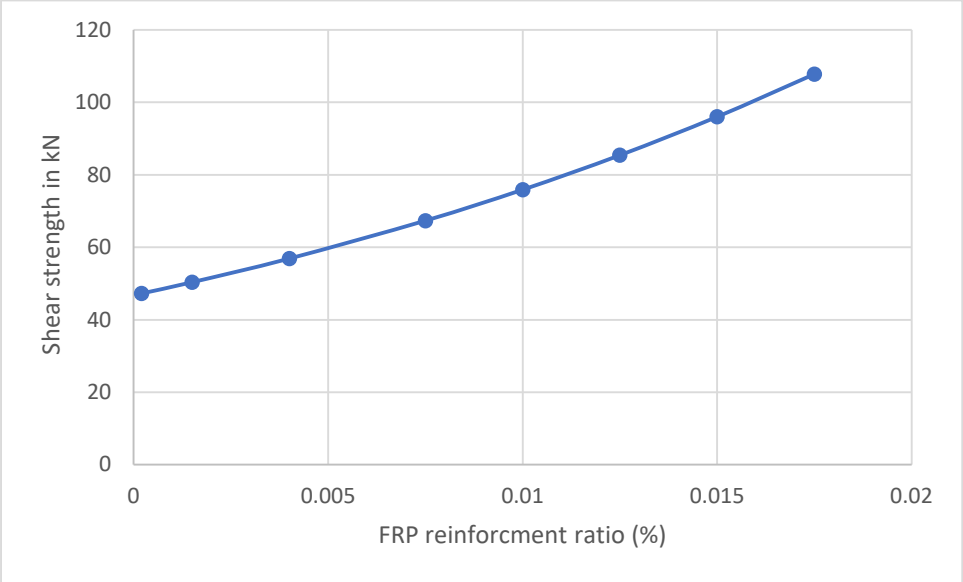

Figure 20. The effect of X14 on the shear strength.

Preprints (www.preprints.org) | NOT PEER-REVIEWED | Posted: 23 August 2022 doi:10.20944/preprints202205.0170.v2

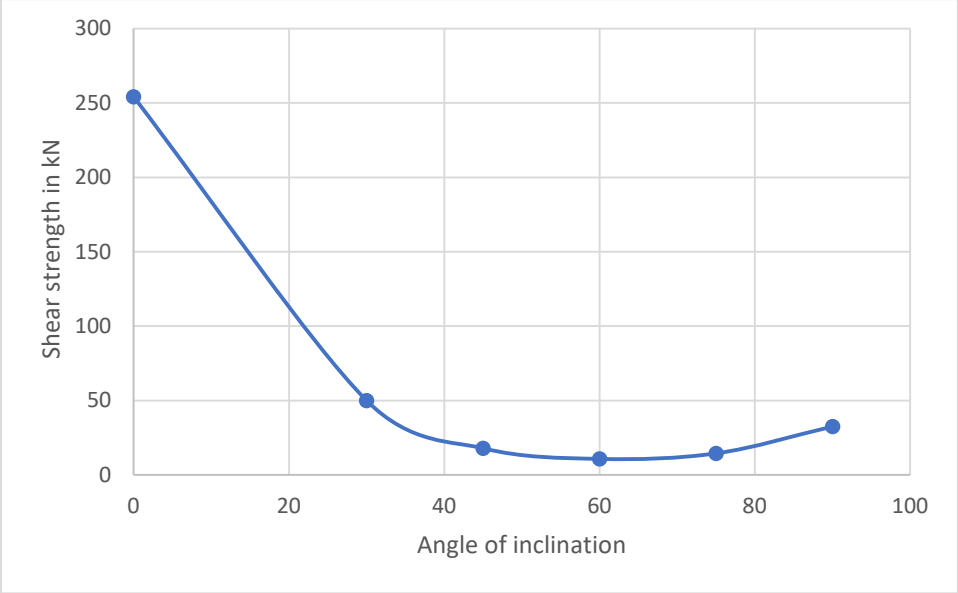

Figure 21. The effect of X15 on shear strength value.

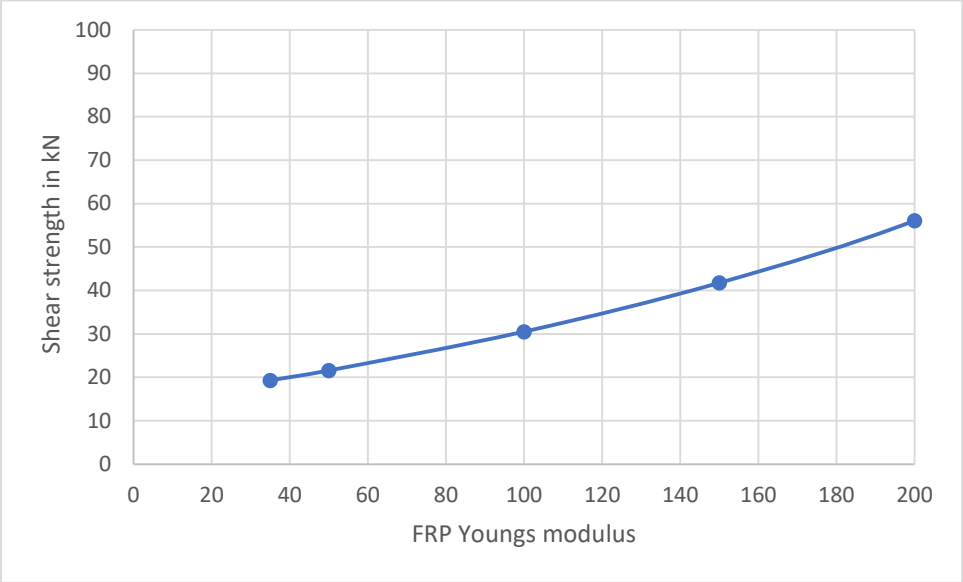

Figure 22. The effect of X17 on shear strength value.

6. Comparisons between the proposed model and existing machine models

In 2020 machine learning was used to predict the FRP shear strength capacity with a certain accuracy [45]. In this work, the proposed model performance has been evaluated and compared to the models from the literature. R^2 is one of the essential statistical parameters that can determine the accuracy of any model regardless of the values of the used data. R^2 for the overall datasets and the number of data used in

Preprints (www.preprints.org) | NOT PEER-REVIEWED | Posted: 23 August 2022 doi:10.20944/preprints202205.0170.v2

developing the new model have been compared with their corresponding values from the previous model, as shown in figure23. The model from this work was constructed using a larger number of dataset points, giving the model a wide range of applicability. In addition, R^2 shows better performance and more accurate results than the models from the literature for all datasets.

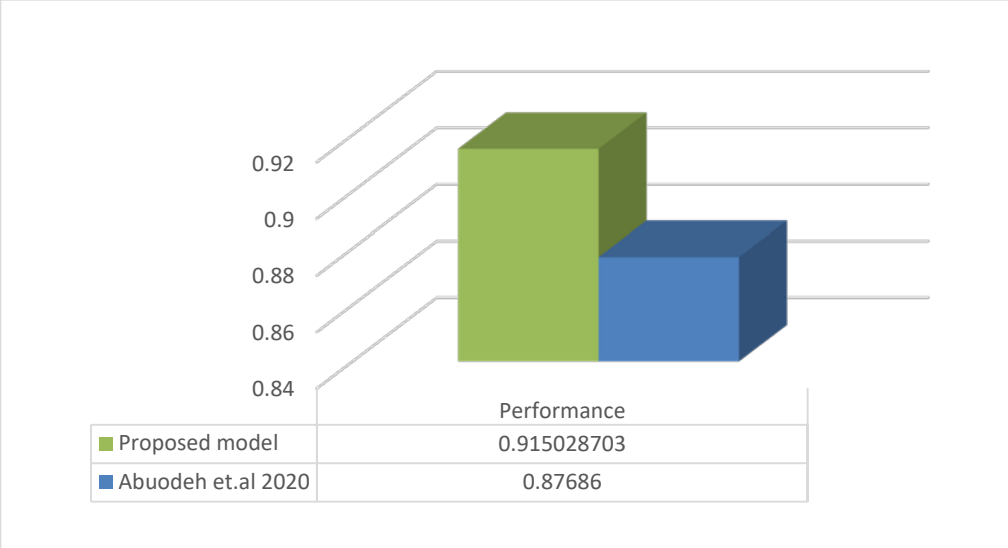

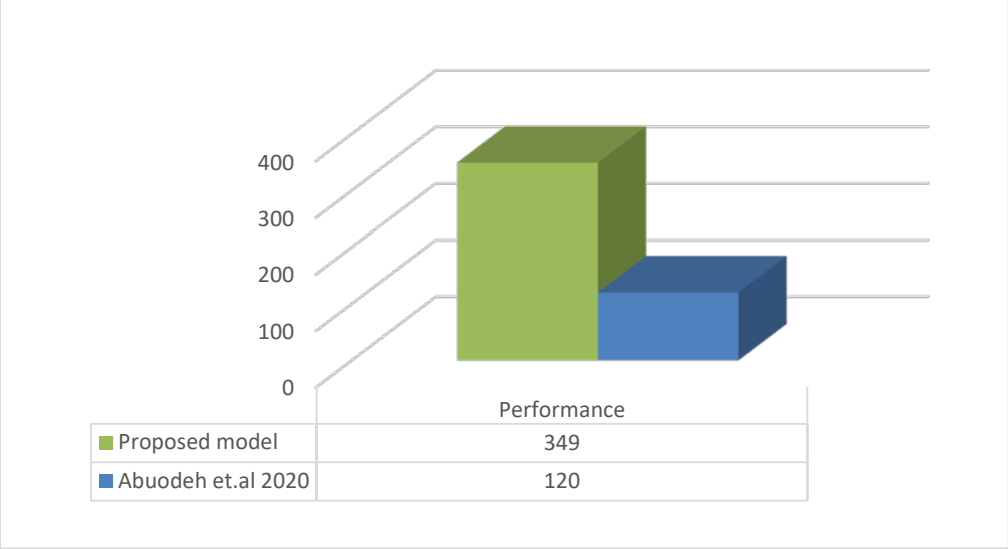

Figure 23. Comparison between the existing models from literature and the proposed model, based on a) R^2 and b) number of data points used.

7. Comparison between the existing design codes and guidelines and the proposed model.

 doi:10.20944/preprints202205.0170.v2

Table 2 shows the statistical measures for various selected models' safety ratios, namely average and coefficient of variation. The safety ratio was defined as the ratio between the measured and the calculated FRP contribution. At the same time, selected models include the proposed model, the Fib 90 [18], the ACI [19], the CNR [20], the TR-55 [21], and the JSCE [22]. The proposed model captured the behavior of FRP strengthened beams and precited the FRP contribution accurately and consistently. The average ranged from 0.98 to 1.14, and the coefficient of variation ranged between 24% to 36%. While the selected models' average ranged between 0.48 to 4.46, and the coefficient of variation ranged between 35% to 95%.

Preprints (www.preprints.org) | NOT PEER-REVIEWED | Posted: 23 August 2022 doi:10.20944/preprints202205.0170.v2

Table 2. Statistical measures for proposed and selected model's a/d ≥ 2.5.

Scheme	Steel stirrups	Continuity	Proposed model		Fib 90		ACI		CNR		TR-55		JSCE	
			SR	C.O.V.	SR	C.O.V.	SR	C.O.V.	SR	C.O.V.	SR	C.O.V.	SR	C.O.V.
Wrapped	Without	Strips	0.98	24%	2.91	49%	3.85	58%	3.00	54%	3.85	58%	1.14	47%
		Continuous	1.14	33%	2.07	38%	-	-	2.15	38%	4.46	59%	0.93	37%
	With	Strips	0.98	24%	1.77	37%	2.32	49%	2.52	42%	2.49	44%	0.88	43%
		Continuous	1.14	33%	0.83	39%	-	-	1.03	43%	1.27	58%	0.43	33%
U-jacket	Without	Strips	1.08	31%	1.50	51%	1.64	64%	1.72	53%	1.58	49%	0.62	46%
		Continuous	1.07	36%	1.12	35%	-	-	1.05	43%	1.07	36%	0.45	36%
	With	Strips	1.08	31%	0.85	87%	1.23	62%	1.20	81%	1.10	68%	0.38	95%
		Continuous	1.07	36%	0.53	45%	-	-	0.51	43%	0.52	46%	0.19	44%
One side	Without	Strips	1.00	29%	-	-	1.34	73%	-	-	1.05	72%	0.74	51%

		Continuous	1.08	30%	-	-	-	-	-	-	0.91	49%	0.84	40%
	With	Strips	1.00	29%	-	-	1.15	72%	-	-	0.71	37%	0.61	47%
		Continuous	1.08	30%	-	-	-	-	-	-	0.41	41%	0.48	52%

8. Conclusions

MATLAB script has been developed to create 6750 different ANN models to compare and optimize the model performance. The model can predict the shear strength added value of FRP knowing the Width of beam cross-section, beam height, the effective depth of beam cross-section, strength technique, FRP jacket height, the width of FRP jacket, the thickness of FRP jacket, spacing between FRP strips, angle of fiber orientation, ultimate stress of FRP, FRP young's modulus, and FRP rupture strain. The input and output data have been adjusted to give a more efficient and faster training process. The model's accuracy has been measured using several statistical tests. R^2, RMSE, ARE, AARE, and SD was found to be 0.91, 17.45, 0.048, 0.23, and 0.91, respectively, for the overall dataset. A parametric study has been conducted to study the influence of the FRP jacket height, the width of the FRP jacket, the thickness of the FRP jacket, spacing between FRP strips, angle of fiber orientation, ultimate stress of FRP, FRP young's modulus, and FRP rupture strain. A comparison between the newly developed model and the model from previous work has been made. The comparison showed that the proposed model has better accuracy, and the number of datasets used in this research is larger than in the other work.

8. Patents

This section is not mandatory but may be added if there are patents resulting from the work reported in this manuscript.

Supplementary Materials: Not applicable.

 doi:10.20944/preprints202205.0170.v2

Author Contributions: Conceptualization, Gasser and Omar.; methodology, Gasser and Omar.; software, Gasser and Omar.; validation, Gasser and Omar.; resources, Deifalla.; data curation, Deifalla.; writing—original draft preparation, Gasser and Omar.; supervision, Deifalla.; project administration.

Funding: This research received no external funding.

Data Availability Statement: Not applicable.

Acknowledgments: Not applicable.

Conflicts of Interest: The authors declare absoluely no conflict in the interest

References

1. Whittle, R. Failures in Concrete Structures—Case Studies in Reinforced and Prestressed Concrete; FL 33487-2742; CRC Press: Boca Raton, FLorida, USA; Taylor and Francis Group, Abingdon, UK, 2013; 140 pp.
2. Chalioris C. E..; Karayiannis C. Effectiveness of the use of Steel fibres on the Torsional behavior of Flanged concrete beams. Cement Concrete Composites. 2009, 31, 331–341.
3. Deifalla A.; Awad A.; Seleem H.; AbdElrahman A. Experimental and Numerical Investigation of the Behavior of LWFC L-girders under Combined torsion. Structures 2020, 26, 362–77. https://doi.org/10.1016/j.istruc.2020.03.070.
4. Deifalla A., Awad A.; Seleem H.; AbdElrahman A. Investigating the Behavior of lightweight foamed concrete T-Beams under Torsion, Shear, and Flexure. Eng. Struct. 2020, 219, 110741. https://doi.org/10.1016/j.engstruct.2020.110741.
5. G. Karayannis, C.; K. Kosmidou, P.-M.; E. Chalioris, C. Reinforced Concrete Beams with Carbon-Fiber-Reinforced Polymer Bars—Experimental Study. Fibers 2018, 6, 99. https://doi.org/10.3390/fib6040099.
6. Gosbell T.; Meggs, R. West gate bridge approach spans FRP strengthening Melbourne. In Proceedings of the IABSE Symposium, Melbourne, Australia, 11–13 September 2002.
7. FIB. FRP Reinforcement in RC Structures; Technical Report Prepared by a Working Party of Task Group 9.3; FIB Bulletin 40; International Federation for Structural Concrete: Lausanne, Switzerland, 2007; p. 151.
8. Oller E., Kotynia R., Antonio Marí A. Assessment of the existing models to evaluate the shear strength contribution of externally bonded frp shear reinforcements. Composite Structures 264 (2021) 113641.https://doi.org/10.1016/j.compstruct.2021.113641.
9. Kotynia, R., Oller, E., Marí, A., Kaszubska, M. Efficiency of shear strengthening of RC beams with externally bonded FRP materials – State-of-the-art in the experimental tests. Composite Structures 267 (2021) 113891. https://doi.org/10.1016/j.compstruct.2021.113891.

10. De Lorenzis, L., and Nanni, A., Shear strength of reinforced concrete beams with FRP rods, J. Comp. Constr., 2001, 5(2), 114–121.
11. Deifalla A. Refining the Torsion Design of Fibered Concrete Beams Reinforced with FRP using Multi-variable Non-linear Regression Analysis for Experimental Results. Eng. Struct. 2020, 224, 111394.
12. Deifalla, A. Torsion Design of Lightweight Concrete Beams without or with Fibers: A comparative study and a refined cracking torque formula. Structures 2020, 28, 786–802. https://doi.org/10.1016/j.istruc.2020.09.004.
13. Deifalla, A. Torsional Behavior of Rectangular and Flanged Concrete Beams with FRP Reinforcements. J. Struct. Eng. 2015, 141, 04015068.
14. Deifalla, A.F.; Zapris, A.G.; Chalioris, C.E. Multivariable Regression Strength Model for Steel Fiber-Reinforced Concrete Beams under Torsion. Materials 2021, 14, 3889. https://doi.org/10.3390/ma14143889.
15. Hassan, M.M.; Deifalla, A. Evaluating the new CAN/CSA-S806-12 torsion provisions for concrete beams with FRP reinforcements. Mater. Struct. 2016, 49, 2715–2729. https://doi.org/10.1617/s11527-015-0680-9.
16. Salem, N.M.; Deifalla, A. Evaluation of the Strength of Slab–Column Connections with FRPs Using Machine Learning Algorithms. Polymers 2022, 14, 1517. https://doi.org/10.3390/polym14081517.
17. Deifalla, A.; Awad, A.; El-Garhy, M. Effectiveness of Externally Bonded CFRP Strips for Strengthening Flanged Beams under Torsion: An Experimental Study. Eng. Struct. 2013, 56, 2065–2075.
18. fib Task group 5.1. FIB Bulletin 90, Externally applied FRP reinforcement for concrete structures. Lausanne, Switzerland: 2019.
19. ACI Committee 440. ACI 440.2R-17, Guide for the Design and Construction of Externally Bonded FRP Systems for Strengthening Concrete Structures. Farmington Hills, Michigan, USA: 2017.
20. Construction C– AC on TR for. CNR-DT 200 R1/2013 Guide for the Design and Construction of Externally Bonded FRP Systems for Strengthening Existing Structures. Rome, Italy: 2013.
21. TR-55 CSTR. Design guidance for strengthening concrete structures using fiber composite materials. London, Great Britain: 2012.

 doi:10.20944/preprints202205.0170.v2

22. JSCE Japanese Society of Civil Engineers. Recommendations for upgrading of concrete structures with use of continuous fiber sheets; 2000.
23. Bousselham A, Chaallal O. Behavior of reinforced concrete t-beams strengthened in shear with carbon fiber-reinforced polymer-an experimental study. ACI Struct J 2006; 103:339–47.
24. Bousselham A, Chaallal O. Mechanisms of shear resistance of concrete beams strengthened in shear with externally bonded FRP. J Compos Constr 2008; 12:499–512. https://doi.org/10.1061/(ASCE)1090-0268(2008)12:5(499).
25. Chen GM, Teng JG, Chen JF, Rosenboom OA. Interaction between steel stirrups and shear strengthening FRP strips in RC beams. J Compos Constr 2010; 14:498–509. https://doi.org/10.1061/(ASCE)CC.1943-5614.0000120.
26. Pellegrino C, Modena C. Fiber reinforced polymer shear strengthening of reinforced concrete beams with transverse steel reinforcement. J Compos Constr 2002; 6:104–11. https://doi.org/10.1061/(ASCE)1090-0268(2002)6:2.
27. Pellegrino C, Vasic M. Assessment of design procedures for the use of externally bonded FRP composites in shear strengthening of reinforced concrete beams. Compos Part B Eng 2013; 45:727–41. https://doi.org/10.1016/j. compositesb.2012.07.039.
28. Sas G, Täljsten B, Barros J, Lima J, Carolin A. Are available models reliable for predicting the FRP contribution to the shear resistance of RC beams. Journal of Compositses for Construction 2009; 13:514–34. https://doi.org/10.1061/(ASCE)CC.1943- 5614.0000045.
29. Mofidi A, Chaallal O. Tests and Design Provisions for Reinforced-Concrete Beams Strengthened in Shear Using FRP Sheets and Strips. Int J Concr Struct Mater 2014; 8:117–28. https://doi.org/10.1007/s40069-013-0060-1.
30. Mofidi A, Chaallal O. Shear strengthening of RC beams with externally bonded FRP composites: effect of strip-width-to-strip-spacing ratio. J Compos Constr 2011; 15:732–42. https://doi.org/10.1061/(ASCE)CC.1943-5614.0000219.

31. Mofidi A, Chaallal O. Shear Strengthening of RC Beams with EB FRP: Influencing Factors and Conceptual Debonding Model. J Compos Constr 2011; 15:62–74. https://doi.org/10.1061/(ASCE)CC.1943-5614.0000153.
32. Kalfat R, Al-Mahaidi R, Smith S. Anchorage devices used to improve the performance of reinforced concrete beams retrofitted with FRP composites: state-of-the-art review. Journal Composites for Construction, 2013;17(1):14–33.
33. Godat A. Hammad F., Chaallal O. State-of-the-art review of anchored FRP shear-strengthened RC beams: A study of influencing factors. 2020. Composite Structures 254 (2020) 112767.
34. Deifalla, A.; Salem, N.M. A Machine Learning Model for Torsion Strength of Externally Bonded FRP-Reinforced Concrete Beams. Polymers 2022, 14, 1824. https://doi.org/10.3390/polym14091824.
35. Colotti V, Swamy RN. Unified analytical approach for determining shear capacity of RC beams strengthened with FRP. Eng Struct 2011; 33:827–42.
36. Sas G, Täljsten B, Barros J, Lima J, Carolin A. Are available models reliable for predicting the FRP contribution to the shear resistance of RC beams? J Compos Constr 2009; 13:514–34. https://doi.org/10.1061/(ASCE)CC.1943-5614.0000045.
37. Kotynia R, Oller E, Mari AR, Kaszubska M. Efficiency of shear strengthening of RC beams with externally bonded FRP materials – State-of-the-art in the experimental tests. Compos Part B Eng n.d.
38. Abuodeh, Omar R., Jamal A. Abdalla, and Rami A. Hawileh. Prediction of shear strength and behavior of RC beams strengthened with externally bonded FRP sheets using machine learning techniques. Composite Structures 234 (2020): 111698.
39. Benzeguir, Z.E.A.; Chaallal, O. Size Effect in FRP Shear-Strengthened RC Beams: Design Models versus Experimental Data. CivilEng 2021, 2, 874-894. doi: 10.3390/civileng2040047
40. Kim, S.-W. Prediction of Shear Strength of Reinforced High-Strength Concrete Beams Using Compatibility-Aided Truss Model. Appl. Sci. 2021, 11, 10585. doi: 10.3390/app112210585

41. Isleem, H.F.; Abid, M.; Alaloul, W.S.; Shah, M.K.; Zeb, S.; Musarat, M.A.; Javed, M.F.; Aslam, F.; Alabduljabbar, H. Axial Compressive Strength Models of Eccentrically-Loaded Rectangular Reinforced Concrete Columns Confined with FRP. Materials 2021, 14, 3498. doi: 10.3390/ma14133498
42. Ly, H.-B.; Le, T.-T.; Vu, H.-L.; Tran, V.Q.; Le, L.M.; Pham, B.T. Computational Hybrid Machine Learning Based Prediction of Shear Capacity for Steel Fiber Reinforced Concrete Beams. Sustainability 2020, 12, 2709. doi: 10.3390/su12072709
43. Chalioris, C.E.; Zapris, A.G.; Karayannis, C.G. U-Jacketing Applications of Fiber-Reinforced Polymers in Reinforced Concrete T-Beams against Shear—Tests and Design. Fibers 2020, 8, 13. doi: 10.3390/fib8020013.